arXiv:nucl-th/0408006v4 10 Oct 2005

Possibility of determining the parity of the pentaquark Θ^+ from photoproduction near threshold

Byung Geel Yu,[1,2,*] Tae Keun Choi,[3,†] and Chueng-Ryong Ji[2,‡]

[1]*Department of General studies, Hankuk Aviation University, Koyang, 412-791, Korea*

[2]*Department of Physics, North Carolina State University, Raleigh, North Carolina 27695-8202, USA*

[3]*Department of Physics, Yonsei University, Wonju, 220-710, Korea*

(Dated: February 8, 2008)

Abstract

We discuss the possibility of determining the parity of the Θ^+ baryon from photoproduction $\gamma N \to K\Theta^+$ process near threshold. We utilize the conservation laws of parity and angular momentum for the analysis of angular distributions and spin observables near threshold. Since the discussion is in essence a partial wave analysis of the production mechanism the result should be less dependent on the model parameters. Our analysis shows that the angular distribution and photon polarization asymmetry for the process of neutron target are sensitive to the parity of the Θ^+, but not for the case of proton target. In the case of proton target, the polarization asymmetries of target and recoiled Θ^+ are preferred for parity determination.

PACS numbers: 13.40.-f, 13.60.Rj, 13.75.Jz, 13.88.+e

Keywords: Θ^+ parity, photoproduction, angular distribution, parity and angular momentum conservations, polarization asymmetry

*Electronic address: bgyu@mail.hangkong.ac.kr

†Electronic address: tkchoi@dragon.yonsei.ac.kr

‡Electronic address: crji@unity.ncsu.edu

I. INTRODUCTION

Experimental evidences for the pentaquark $\Theta^+(1540)$ [1] have been debated since the first claim of observing the narrow peak in the LEPS collaboration at SPring-8 [2]. In a sequence of the following experiments, more than 10 experiments reported affirmative results on the existence of the Θ^+ [3, 4]. However, many other experiments, in particular, those performed using e^+e^- processes and high energy proton beams could not support the existence of Θ^+ [5]. Recent report from the CLAS collaboration in the g_{11} experiment [6] is especially disturbing since it refutes the earlier SAPHIR experiment [3]. Nevertheless, the existence of the pentaquark Θ^+ has not yet been ruled out [7, 8] due to the limited experimental factors such as low statistics, uncertainty in the background effect, and the specific cuts in angle for data analysis. We think that more refined experiments are crucial to resolve this debate and further analyses on the Θ^+ system would be worthwhile till the debate is resolved.

In theoretical side, it is crucial to determine the parity of the Θ^+ because the parity is a decisive quantum number to understand its substructure with strangeness $S = +1$ [9, 10]. In Ref. [11] and in subsequent works [12, 13], the conservation laws were applied to give strong constraints on the parity and angular momentum of the initial pp state in the polarized process $pp \to \Sigma^+\Theta^+$ near threshold. These works claimed that the parity of the Θ^+ can be clearly determined by the Fermi statistics of a two-nucleon system. Also, Ref. [14] suggested that the parity of the Θ^+ can be determined model-independently by observing the polarization asymmetries based on the reflection symmetry in the polarized process of $\gamma N \to K\Theta^+$. In addition, Refs. [15, 16, 17] proposed to use a polarized photon beam for the process $\gamma N \to K\Theta^+$ to determine the Θ^+ parity model-independently. These works emphasize that the polarization observables are important tools to determine the Θ^+ parity.

In this work, we discuss a possibility that the conservation laws of parity and angular momentum for the *unpolarized* observable can also be exploited to determine the parity of the Θ^+ in the photoproduction process, if the photon energy lies near threshold. We present in detail the role of parity and angular momentum conservation on the process $\gamma N \to K\Theta^+$ and show that it is possible to describe the amplitude of the process near threshold from first principles with the threshold kinematics. As a result, the two assumed states of the Θ^+ corresponding to each parity can be distinguished from each other by analyzing simply the angular distribution of the unpolarized photoproduction process. In the same line of reasoning we can also extend this sort of analysis to the polarized process and make a prediction for the polarization asymmetries of the photon beam

(or of the target) and the recoiled Θ^+. Similar type of analysis for the photoproduction process has already been applied to pion photo and electroproduction processes near threshold [18, 19, 20]. The analogy of the charge coupling structures between the processes $\gamma n \to K^- \Theta^+ (\gamma p \to \bar{K}^0 \Theta^+)$ and $\gamma n \to \pi^- p (\gamma p \to \pi^0 p)$ is useful for our analysis.

For explicit quantitative predictions, we present numerical results of the angular distribution and single polarization asymmetries using the hadron model in Ref. [21]. The model dependence in this case, however, can be minimized near threshold because the conservation laws can be implemented only to the lower states of angular momentum available near threshold.

In Section 2, we present our reasoning for the difference in the angular distribution depending on the parity of the Θ^+ rather than total cross section. The conservation laws of parity and angular momentum are applied for identifying the leading multipole in the photoproduction of the positive and negative parity of the Θ^+. The CGLN amplitudes based on the threshold kinematics are also used for discussing consistency of our description. Numerical estimations follow for illustration. Section 3 is devoted to the analysis of the angular distribution and single polarization observables with respect to the parity of Θ^+. Summary and discussion follow in Section 4.

II. CONSERVATION LAWS AND THRESHOLD KINEMATICS

Before we proceed to analyze the angular distribution of $\gamma N \to K \Theta^+$ based on the conservation laws of the parity and angular momentum, we first start with a summary of our reasoning why the total cross sections alone may not be so effective in determining the Θ^+ parity.

Fig. 1 shows the cross sections for $\gamma N \to K \Theta^+$ obtained from our previous work [21] with the coupling constant $g_{KN\Theta}$ taken from the width $\Gamma_\Theta = 1$ MeV for both parities [22]. Following Refs. [23, 24, 25], the coupling constant K^* and subsequently that of K_1 have been updated as $g_{K^*N\Theta} = \sqrt{3} g_{KN\Theta}$ for the positive parity, and $g_{K^*N\Theta} = \frac{1}{\sqrt{3}} g_{KN\Theta}$ for the negative parity of the Θ^+, respectively. The tensor coupling constants of the K^* and K_1 are also neglected to avoid unnecessary complication in our analysis near threshold. The coupling constants used in the calculation are listed in Table I.

While the reanalysis of the SAPHIR data lowered the magnitude of the total cross section of $\gamma p \to \bar{K}^0 \Theta^+$ from initially 300 nb to around 50 nb, the most recent analysis from the CLAS collaboration reported even further reduction with an upper bound of $1 \sim 4$ nb at most [6]. As can be seen in Fig. 1, our total cross section of the $\gamma p \to \bar{K}^0 \Theta^+$ process for the case of negative parity Θ^+(Fig. 1(d)) seems now to agree with the recent CLAS analysis. However, our total cross section

TABLE I: Coupling constants used in the calculation for $\gamma N \to K\Theta^+$. $\Gamma_{\Theta^+\to NK} = 1$ MeV taken for $g_{KN\Theta}$ of the $\Theta^+(\frac{1}{2}^\pm)$ [22]. Superscripts a, b, c and d in the last column of References denote ^{a}the assumption [23, 24, 25], ^{b}PDG [26], $^c\gamma p \to K^+\Lambda$ [27] with assumption $\frac{G_{K^*N\Theta}}{G_{K_1N\Theta}} \simeq \frac{G_{K^*N\Lambda(1116)}}{G_{K_1N\Lambda(1116)}}$ for $\Theta^+(\frac{1}{2}^+)$ and $\frac{G_{K^*N\Theta}}{G_{K_1N\Theta}} \simeq \frac{G_{K^*N\Lambda(1405)}}{G_{K_1N\Lambda(1405)}}$ for $\Theta^+(\frac{1}{2}^-)$ with $G_{K^*(K_1)NY} = g_{K^*(K_1)K\gamma}g_{K^*(K_1)NY}$, and $^d\Gamma_{K_1K\rho} = 37.8$ MeV with Vector Meson Dominance $g_{K_1K\gamma} = \frac{e}{f_\rho}g_{K_1K\rho}$ [28]. Values in the parenthesis denote $\gamma n \to K^-\Theta^+(\gamma p \to \bar{K}^0\Theta^+)$ respectively.

	Positive parity	Negative parity	References
$g_{KN\Theta}$	0.984	0.137	$\Gamma_{\Theta^+\to NK}$
$g_{K^*N\Theta}$	$\pm$1.704	$\pm$0.08	$\frac{g_{K^*N\Theta}}{g_{KN\Theta}} = \sqrt{3}, (\frac{1}{\sqrt{3}})^a$
$g_{K^*K\gamma}$	0.254(0.388)	0.254(0.388)	$\Gamma_{K^*\to K\gamma}{}^b$
$g_{K_1N\Theta}$	$\mp$ 0.09(0.138)		$\frac{G_{K^*N\Lambda(1116)}}{G_{K_1N\Lambda(1116)}} \simeq -8^c$
		$\mp$0.048(0.074)	$\frac{G_{K^*N\Lambda(1405)}}{G_{K_1N\Lambda(1405)}} \simeq -0.7^c$
$g_{K_1K\gamma}$	0.6	0.6	$g_{K_1K\rho}{}^d$

can change to agree with the SAPHIR data (50 nb) if the decay width $\Gamma_\Theta = 5$ MeV is taken as in the case of earlier analysis. Moreover, the CLAS measurements and the SPring8 measurements [8] have been exclusive to each other in the sense that the SPring8 measurements were limited only to the forward direction of the produced particles but the CLAS measurements excluded this forward direction entirely. Therefore, although our results for the photoproduction of the negative parity Θ^+ using the proton target are consistent with the most recent CLAS data, a definite conclusion from the total cross section cannot be made until the improvement is made to match kinematic regions between the two facilities.

It is, thus, necessary to go beyond the total cross sections and investigate angular distributions and possibly other observables for discriminating the Θ^+ parity [21]. Although the hadron model involves several unknown parameters, we expect that such model dependence can be minimized in the analysis near threshold because only the lower angular momentum states are available and thus it is rather easy to implement the first principle conservation laws [11].

In the threshold region it is legitimate to assume that the angular momentum of kaon is $l = 0$ or 1 in the final $K\Theta^+$ state, because a typical hadronic scale R is one fermi and $|\boldsymbol{q}|R \approx \sqrt{l(l+1)} \leq 2$ up to a few hundred MeV/c of the kaon momentum $|\boldsymbol{q}|$ in the center of mass(CM) frame. The angular momentum of the final state is therefore either $J = \frac{1}{2}$ or $\frac{3}{2}$. The parity of the final state is given by $(-1)^{l+1}$ for the positive parity of the $\Theta^+(\frac{1}{2}^+)$, and by $(-1)^l$ for the negative parity of the

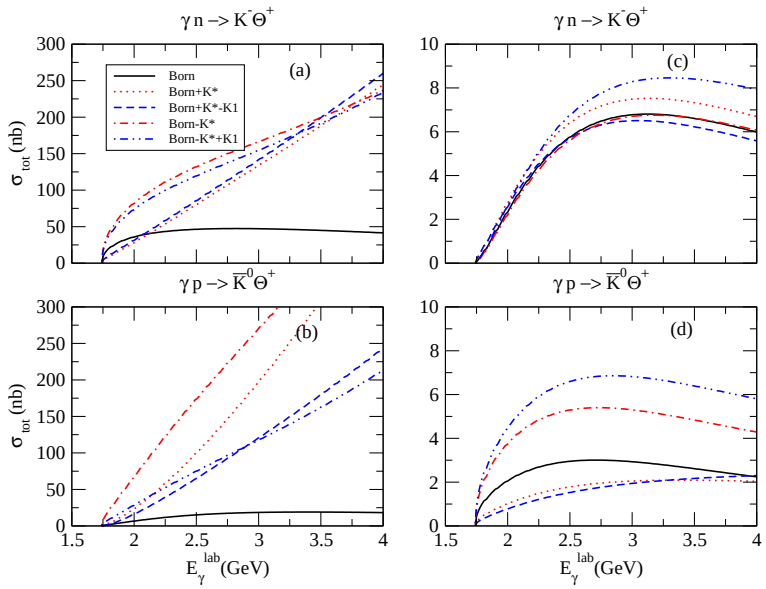

FIG. 1: Total cross sections of the $\gamma N \to K\Theta^+$ in the PV coupling scheme. Panels (a) and (b) ((c) and (d)) are for $\Theta^+(\frac{1}{2}^+)$ ($\Theta^+(\frac{1}{2}^-)$). The solid lines are the contributions of the Born terms with $g_{KN\Theta} = 0.984(0.137)$ and $g_{K^*N\Theta} = 0$, $g_{K_1N\Theta} = 0$. The dotted lines are the sum of the Born terms and K^* contribution with $g_{K^*N\Theta} = 1.704(0.08)$. The dot-dashed lines are the sum of the Born terms and K^* with $g_{K^*N\Theta} = -1.704(-0.08)$. The dashed lines are the sum of the Born terms, K^* and K_1 contributions with $g_{K^*N\Theta} = 1.704$, $g_{K_1N\Theta} = -0.09(-0.138)$ for $\gamma n \to K^-\Theta^+(\gamma p \to \bar{K}^0\Theta^+)$ for $\Theta^+(\frac{1}{2}^+)$ and $g_{K^*N\Theta} = 0.08$, $g_{K_1N\Theta} = -0.048(-0.074)$ for $\gamma n \to K^-\Theta^+(\gamma p \to \bar{K}^0\Theta^+)$ for $\Theta^+(\frac{1}{2}^-)$. The dot-dot-dashed lines are the sum of the Born terms, K^* and K_1 contributions with $g_{K^*N\Theta} = -1.704$, $g_{K_1N\Theta} = +0.09(+0.138)$ for $\gamma n \to K^-\Theta^+(\gamma p \to \bar{K}^0\Theta^+)$ for $\Theta^+(\frac{1}{2}^+)$ and $g_{K^*N\Theta} = -0.08$, $g_{K_1N\Theta} = +0.048(+0.074)$ for $\gamma n \to K^-\Theta^+(\gamma p \to \bar{K}^0\Theta^+)$ for $\Theta^+(\frac{1}{2}^-)$.

$\Theta^+(\frac{1}{2}^-)$. The angular momentum of the initial γN state is given by $J = |L \pm \frac{1}{2}|$, where L is the total orbital angular momentum of the photon [18]. For transverse photon, the parity of the initial state can have either $(-1)^L$ for electric, or $(-1)^{L+1}$ for magnetic states of the photon [18, 19]. Then, from the conservation of parity and angular momentum, only s- and p-waves are allowed, as summarized in Table II. Near threshold, however, the electric transition must be dominant over the magnetic transition. Also the lower state of J(i.e., $J = \frac{1}{2}$) must be energetically more accessible than the higher state of J(i.e., $J = \frac{3}{2}$). Therefore, the dominant transitions near threshold are E_{0+} for the $\Theta^+(\frac{1}{2}^+)$, and E_{1-} for the $\Theta^+(\frac{1}{2}^-)$, respectively. This would make a clear distinction between the two angular distributions for the $\gamma N \to K\Theta^+$ process, depending on the Θ^+ parity. In this work we show that this expectation generally holds for the case of $\gamma n \to K^-\Theta^+$, while the case of $\gamma p \to \bar{K}^0\Theta^+$ does not share the same features due to the absence of the charge coupling of

TABLE II: Multipole states for $\gamma N \to K\Theta^+$. For the transverse photon states, $L \geq 1$. The angular momentum $J = |l \pm \frac{1}{2}| = |L \pm \frac{1}{2}|$. From the parity conservation for $\Theta^+(\frac{1}{2}^+)$ EL : $(-1)^L = (-1)^{l+1}$, ML : $(-1)^{L+1} = (-1)^{l+1}$. For $\Theta^+(\frac{1}{2}^-)$ EL : $(-1)^L = (-1)^l$, ML : $(-1)^{L+1} = (-1)^l$.

	Positive parity				Negative parity			
L	EL(ML)	J^P	l	multipoles	EL(ML)	J^P	l	multipoles
1	E1	$\frac{1}{2}^-$	0	E_{0+}	M1	$\frac{1}{2}^+$	0	M_{0+}
1	M1	$\frac{1}{2}^+$	1	M_{1-}	E1	$\frac{1}{2}^-$	1	E_{1-}
1	M1	$\frac{3}{2}^+$	1	M_{1+}	E1	$\frac{3}{2}^-$	1	E_{1+}
2	E2	$\frac{3}{2}^+$	1	E_{1+}	M2	$\frac{3}{2}^-$	1	M_{1+}

photon to neutral $\bar{K}^0$ meson.

A. Consistency with CGLN Amplitudes

To check the consistency of our description, let us now expand the photoproduction current in terms of CGLN amplitudes [29]. In the case of $\Theta^+(\frac{1}{2}^+)$, the CGLN expansion is given by

$$\boldsymbol{J}^+ \cdot \hat{\boldsymbol{\epsilon}}_\lambda = F_1^+ \, i\boldsymbol{\sigma} \cdot \hat{\boldsymbol{\epsilon}}_\lambda + F_2^+ \, \boldsymbol{\sigma} \cdot \hat{\boldsymbol{q}} \, \boldsymbol{\sigma} \cdot (\hat{\boldsymbol{k}} \times \hat{\boldsymbol{\epsilon}}_\lambda) + F_3^+ \, i\boldsymbol{\sigma} \cdot \hat{\boldsymbol{k}} \, \hat{\boldsymbol{q}} \cdot \hat{\boldsymbol{\epsilon}}_\lambda + F_4^+ \, i\boldsymbol{\sigma} \cdot \hat{\boldsymbol{q}} \, \hat{\boldsymbol{q}} \cdot \hat{\boldsymbol{\epsilon}}_\lambda, \tag{1}$$

where $\hat{\boldsymbol{k}}$ and $\hat{\boldsymbol{q}}$ are unit vectors of photon and kaon three momenta, respectively, and $\hat{\boldsymbol{\epsilon}}_\lambda$ is the photon polarization vector with the polarization λ. Likewise, the expansion of photoproduction current for the $\Theta^+(\frac{1}{2}^-)$ is given by [30]

$$\boldsymbol{J}^- \cdot \hat{\boldsymbol{\epsilon}}_\lambda = F_1^- \, i\boldsymbol{\sigma} \cdot (\hat{\boldsymbol{k}} \times \hat{\boldsymbol{\epsilon}}_\lambda) + F_2^- \, \boldsymbol{\sigma} \cdot \hat{\boldsymbol{q}} \, \boldsymbol{\sigma} \cdot \hat{\boldsymbol{\epsilon}}_\lambda + F_3^- \, i\boldsymbol{\sigma} \cdot (\hat{\boldsymbol{q}} \times \hat{\boldsymbol{k}}) \, \hat{\boldsymbol{q}} \cdot \hat{\boldsymbol{\epsilon}}_\lambda + F_4^- \, \hat{\boldsymbol{q}} \cdot \hat{\boldsymbol{\epsilon}}_\lambda \, . \tag{2}$$

Here and in what follows, the superscripts $\pm$ stand for the two possible parities of the Θ^+. The CGLN amplitudes in Eqs. (1) and (2) are given by

$$\begin{aligned}
F_1^\pm &= \pm \frac{|\boldsymbol{k}|}{4\pi} N_+ \left[A_1^\pm \mp \frac{1}{2}(W \pm M) A_3^\pm \mp \frac{p' \cdot k}{W \mp M} A_4^\pm \right], \\
F_2^\pm &= \pm \frac{|\boldsymbol{k}|}{4\pi} N_- \left[A_1^\pm \pm \frac{1}{2}(W \mp M) A_3^\pm \pm \frac{p' \cdot k}{W \pm M} A_4^\pm \right], \\
F_3^\pm &= \mp \frac{|\boldsymbol{k}||\boldsymbol{q}|}{4\pi} N_\pm \left[(W - M) A_2^\pm - A_4^\pm \right], \\
F_4^\pm &= \pm \frac{|\boldsymbol{k}||\boldsymbol{q}|}{4\pi} N_\mp \left[(W + M) A_2^\pm + A_4^\pm - \frac{(W + M)\boldsymbol{k} \cdot \boldsymbol{q}}{(E + M)(E_\Theta + M_\Theta)} \left(A_2^- - \frac{A_4^-}{W - M} \right) \right],
\end{aligned} \tag{3}$$

with the normalization constants $N_\pm = \sqrt{\frac{E_\Theta \pm M_\Theta}{2W}}$.

We now note that, regardless of any model descriptions for $A_i^{\pm}$, essentially the knowledge of the kinematics near threshold enables us to determine which amplitude in the CGLN expansion of Eqs.(1) and (2) gives the leading contribution to the currents $\boldsymbol{J}^{\pm}$. First, the amplitudes F_2^+ and F_4^+ in Eq.(1) are substantially suppressed near threshold due to the kinematic constant N_-. Therefore, the current given by Eq.(1) near threshold can be written as $\boldsymbol{J}^+ \cdot \hat{\boldsymbol{\epsilon}}_\lambda \simeq F_1^+ \, i\boldsymbol{\sigma} \cdot \hat{\boldsymbol{\epsilon}}_\lambda + F_3^+ \, i\boldsymbol{\sigma} \cdot \hat{\boldsymbol{k}}\, \hat{\boldsymbol{q}} \cdot \hat{\boldsymbol{\epsilon}}_\lambda$. Similarly, the amplitudes F_2^- and F_3^- are negligible near threshold by the same reason and thus the current in Eq.(2) can be given by $\boldsymbol{J}^- \cdot \hat{\boldsymbol{\epsilon}}_\lambda \simeq F_1^- \, i\boldsymbol{\sigma} \cdot (\hat{\boldsymbol{k}} \times \hat{\boldsymbol{\epsilon}}_\lambda) + F_4^- \, \hat{\boldsymbol{q}} \cdot \hat{\boldsymbol{\epsilon}}_\lambda$.

For the case of the $\Theta^+(\frac{1}{2}^+)$, it is apparent that near threshold the $F_1^+ \, i\boldsymbol{\sigma} \cdot \hat{\boldsymbol{\epsilon}}_\lambda$ is dominant over the $F_3^+ \, i\boldsymbol{\sigma} \cdot \hat{\boldsymbol{k}}\, \hat{\boldsymbol{q}} \cdot \hat{\boldsymbol{\epsilon}}_\lambda$ due to the dominance of the electric transition over the magnetic transition near threshold, viz., $L = 1$ in Table II. Note that the $i\boldsymbol{\sigma} \cdot \hat{\boldsymbol{\epsilon}}_\lambda$ term governs the s-wave multipole of outgoing kaon via electric transition while the $i\boldsymbol{\sigma} \cdot \hat{\boldsymbol{k}}\, \hat{\boldsymbol{q}} \cdot \hat{\boldsymbol{\epsilon}}_\lambda$ term does the p-wave multipole via magnetic transition. For the $\Theta^+(\frac{1}{2}^-)$, however, there is a turnover between the electric and magnetic transitions according to the change of the positive parity of the Θ^+ to the negative one, as shown in Table II. The $i\boldsymbol{\sigma} \cdot (\hat{\boldsymbol{k}} \times \hat{\boldsymbol{\epsilon}}_\lambda)$ term governs the s-wave multipole via magnetic transition, while the $\hat{\boldsymbol{q}} \cdot \hat{\boldsymbol{\epsilon}}_\lambda$ does the p-wave one via electric transition. Thus, in identifying the leading multipole in the CGLN amplitudes for the case of $\Theta^+(\frac{1}{2}^-)$, there is a subtle difference between the $\gamma n \to K^- \Theta^+$ and $\gamma p \to \bar{K}^0 \Theta^+$ processes[1]. Although one expects that $F_4^- \hat{\boldsymbol{q}} \cdot \hat{\boldsymbol{\epsilon}}_\lambda$ be dominant over $F_1^- i\boldsymbol{\sigma} \cdot (\hat{\boldsymbol{k}} \times \hat{\boldsymbol{\epsilon}}_\lambda)$ on account of the dominance of the electric transition over the magnetic transition near threshold, this is fulfilled only in the $\gamma n \to K^- \Theta^+$ of the negative parity Θ^+ but not in the $\gamma p \to \bar{K}^0 \Theta^+$. In case of the latter process, both the s-wave multipoles, $F_1^+ \, i\boldsymbol{\sigma} \cdot \hat{\boldsymbol{\epsilon}}_\lambda$ and $F_1^- i\boldsymbol{\sigma} \cdot (\hat{\boldsymbol{k}} \times \hat{\boldsymbol{\epsilon}}_\lambda)$, are the leading ones to both cases of the Θ^+ parities near threshold due to the absence of the t-channel kaon exchange from the neutralness of $\bar{K}^0$. The electric transition governed by the $F_4^- \hat{\boldsymbol{q}} \cdot \hat{\boldsymbol{\epsilon}}_\lambda$ term, thus, cannot play a dominant role in the case of the $\gamma p \to \bar{K}^0 \Theta^+$ process. On the other hand, one also needs to take into account the fact that $F_1^- i\boldsymbol{\sigma} \cdot (\hat{\boldsymbol{k}} \times \hat{\boldsymbol{\epsilon}}_\lambda)$ is suppressed and becomes smaller than $F_4^- \hat{\boldsymbol{q}} \cdot \hat{\boldsymbol{\epsilon}}_\lambda$ near threshold in the case of $\gamma n \to K^- \Theta^+$ [30, 31]. Such a suppression of magnetic transition near threshold in the case of $F_1^- i\boldsymbol{\sigma} \cdot (\hat{\boldsymbol{k}} \times \hat{\boldsymbol{\epsilon}}_\lambda)$ can be checked by its kinematic factor

[1] It is, of course, true that at threshold $E_\gamma = 1.75$ GeV where $|\boldsymbol{q}| = 0$ exactly only the s-wave multipole $F_1^{\pm}$ survives in any cases [15, 16]. Note that, however, the energy region we are concerned with is the region, slightly above threshold, $E_\gamma = 1.8$ GeV which allows the nonvanishing kaon momentum. Therefore in this region the magnetic dipole transition by small kaon momentum is dominated by the electric one.

of $\frac{|\boldsymbol{k}|}{E+M}$ [2], which makes F_1^- by an order of magnitude smaller than F_1^+, even compared with the positive parity in the same process.

Summarizing above, we thus identify the leading contribution to the currents in Eqs.(1) and (2) as,

$$\begin{aligned} \boldsymbol{J}^+ \cdot \hat{\boldsymbol{\epsilon}}_\lambda &\simeq F_1^+ \, i\boldsymbol{\sigma} \cdot \hat{\boldsymbol{\epsilon}}_\lambda \,, \\ \boldsymbol{J}^- \cdot \hat{\boldsymbol{\epsilon}}_\lambda &\simeq F_4^- \, \hat{\boldsymbol{q}} \cdot \hat{\boldsymbol{\epsilon}}_\lambda \,, \end{aligned} \tag{4}$$

for $\gamma n \to K^- \Theta^+$ [17] and

$$\begin{aligned} \boldsymbol{J}^+ \cdot \hat{\boldsymbol{\epsilon}}_\lambda &\simeq F_1^+ \, i\boldsymbol{\sigma} \cdot \hat{\boldsymbol{\epsilon}}_\lambda \,, \\ \boldsymbol{J}^- \cdot \hat{\boldsymbol{\epsilon}}_\lambda &\simeq F_1^- \, i\boldsymbol{\sigma} \cdot (\hat{\boldsymbol{k}} \times \hat{\boldsymbol{\epsilon}}_\lambda) \,, \end{aligned} \tag{5}$$

for $\gamma p \to \bar{K}^0 \Theta^+$ [15], respectively near threshold. These observations are consistent with our previous discussion based on the conservation laws listed in Table II.

B. Numerical Check

For numerical illustration, we estimate the dependence of CGLN amplitudes $F_i^\pm$ on the energy and angle using the hadron model in Ref. [21] with coupling constants given in Table I and the invariant amplitudes $A_i^\pm$ of the pseudovector(PV) coupling scheme given by

$$\begin{aligned} A_1^\pm &= e g_{KN\Theta} \left[\frac{F_1(s)(\frac{1}{2}(1+\tau_3)+\kappa_N)}{s-M^2} + \frac{F_2(u)(1 \pm \kappa_\Theta)}{u - M_\Theta^2 + i\Gamma_\Theta M_\Theta} \right] \pm \frac{e g_{KN\Theta}}{M_\Theta \pm M} \left(F_1(s)\frac{\kappa_N}{2M} + F_2(u)\frac{\kappa_\Theta}{2M_\Theta} \right) \\ &\quad + \frac{G_V^{K^*}}{m} F_3(t)(M \pm M_\Theta)\Delta_{K^*}, \\ A_2^\pm &= \frac{-2 e g_{KN\Theta}\, \widehat{F}}{X(u - M_\Theta^2 + i\Gamma_\Theta M_\Theta)}\, \tau_3, \\ A_3^\pm &= \frac{e g_{KN\Theta}\, F_1(s)}{s-M^2}\frac{\kappa_N}{M} + \frac{G_V^{K^*}}{m} F_3(t)\Delta_{K^*} \pm \frac{G_V^{K_1}}{m} F_3(t)\Delta_{K_1}, \\ A_4^\pm &= \frac{e g_{KN\Theta}\, F_2(u)}{u - M_\Theta^2 + i\Gamma_\Theta M_\Theta}\frac{\kappa_\Theta}{M_\Theta} + \frac{G_V^{K^*}}{m} F_3(t)\Delta_{K^*} \mp \frac{G_V^{K_1}}{m} F_3(t)\Delta_{K_1} \,. \end{aligned} \tag{6}$$

[2] The nonrelativistic reduction of the vertex $KN\Theta^+(\frac{1}{2}^-)$ in the CM frame yields,

$$V_{KN\Theta} = \frac{e g}{M_\Theta - M}\bar{u}(p')\not{\epsilon} u(p) = \frac{e g}{M_\Theta - M} NN' \frac{|\boldsymbol{k}|}{E+M} \chi^\dagger i\boldsymbol{\sigma} \cdot (\hat{\boldsymbol{k}} \times \hat{\boldsymbol{\epsilon}}_\lambda)\chi + \cdots$$

with $N(N')$ the normalization constant of initial(final) Dirac spinor. At the photon energy E_γ=1.8 GeV in the lab. frame, the kinematic factor $\frac{k}{E+M} \simeq 0.37$ in the CM frame.

Here $F_1(s)$ and $F_2(u)$ are hadronic form factors in the s- and u-channel, respectively, $\widehat{F}$ is a subtraction function to restore gauge invariance of the process and $F_3(t)$ is the vertex form factor for the t-channel meson exchanges including K^* and K_1. In Eq. (6), the anomalous magnetic moments of proton and neutron are $\kappa_p = 1.79$ and $\kappa_n = -1.91$, respectively. Also the factor X in Eq. (6) is given by $X = (s - M^2)$ for $\gamma p \to \bar{K}^0\Theta^+$, and $X = (t - m_K^2)$ for $\gamma n \to K^-\Theta^+$, respectively. Since our calculations show that the results near threshold are not quite sensitive to the value of the Θ^+ anomalous magnetic moment, we take $\kappa_\Theta = 0$ for simplicity. For K^* and K_1 exchanges in the t-channel, the coupling constants are $G_V^{K^*} = g_{\gamma KK^*} g_{K^*N\Theta}$ and $G_V^{K_1} = g_{\gamma KK_1} g_{K_1N\Theta}$ with a parameter of mass dimension, m and the propagators, $\Delta_{K^*(K_1)} = [t - m^2_{K^*(K_1)} + i\Gamma_{K^*(K_1)} m_{K^*(K_1)}]^{-1}$ [21].

Figs. 2 and 3 show the results of the CGLN amplitudes in Eq.(3) with $g_{K*N\Theta} = 0$ and $g_{K_1N\Theta} = 0$. Addition of the K^* and K_1 contributions to Eq.(3) cannot alter significantly the leading order amplitude among $F_i^{\pm}$'s as shown in the figures at $E_\gamma = 1.8$ GeV. In Fig. 2, the features of $\gamma n \to K^-\Theta^+$ at $E_\gamma = 1.8$ GeV are represented as a dominance of F_1^+ in the $\Theta^+(\frac{1}{2}^+)$ and F_4^- in the $\Theta^+(\frac{1}{2}^-)$, respectively(see the similar conclusion on the $\gamma n \to K^-\Theta^+$ process in Ref. [16]). Note that Fig. 2 reproduces the suppression of F_1^- by an order of magnitude in comparison with F_1^+. In Fig. 3 one can see that F_1^+ and F_1^- are the leading amplitudes at $E_\gamma = 1.8$ GeV to the $\gamma p \to \bar{K}^0\Theta^+$ process. Therefore, in the threshold region, these figures seem to support our discussions given above, although estimated by the model-dependent calculation.

Before closing this section it is worth noting that Ref. [15] also discussed contributions of partial waves in determining the Θ^+ parity from the $\gamma N \to K\Theta^+$ process.

However, since they did not consider a suppression by a kinematical factor such as $\frac{k}{E+M} \approx 0.37$ which is important in the analysis of the $\gamma n \to K^-\Theta^+$ process near threshold, they started with the s-wave amplitude common to both parities of the Θ^+. Thus, they need to observe spin observables more than single and double polarizations instead of the unpolarized ones, or to use a depolarization tensor component for relating the spin observables with unpolarized cross sections for the model-independent analysis. This makes their results different from ours in the case of $\gamma n \to K^-\Theta^+$.

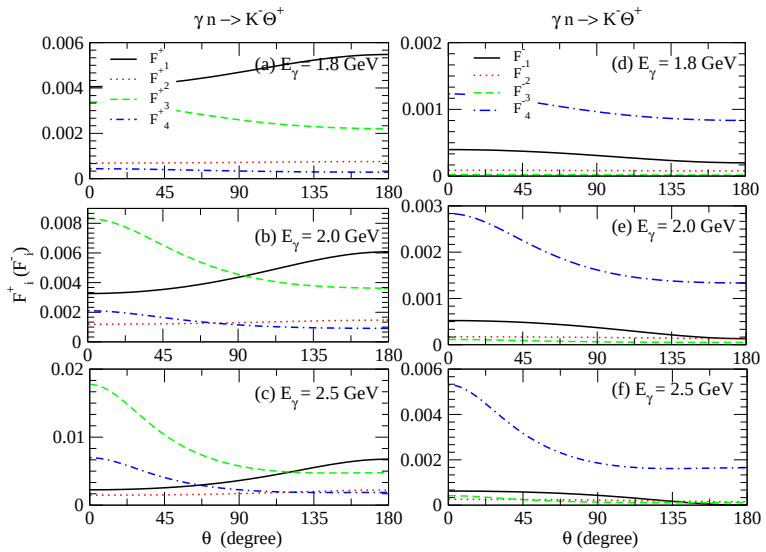

FIG. 2: (Color online) Angle and energy dependence of the CGLN amplitudes F_i^+'s for the $\Theta^+(\frac{1}{2}^+)$((a),(b),(c)) and F_i^-'s for the $\Theta^+(\frac{1}{2}^-)$((d),(e),(f)) in the $\gamma n \to K^-\Theta^+$.

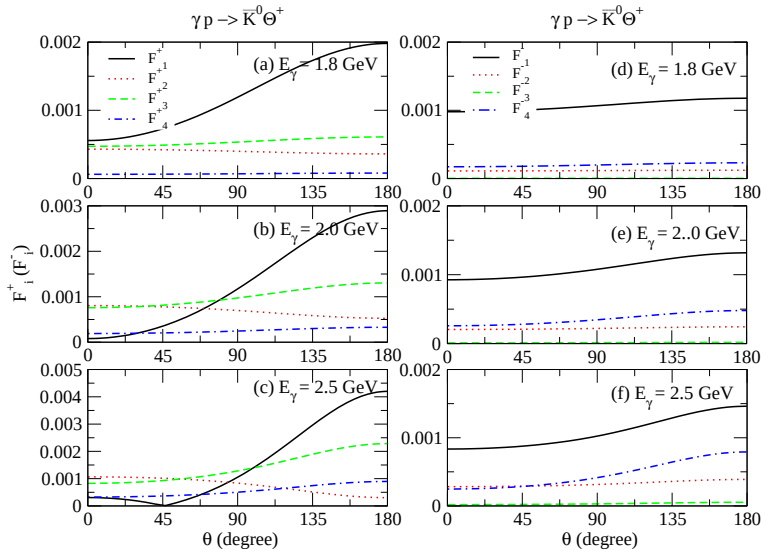

FIG. 3: (Color online) Angle and energy dependence of the amplitudes F_i^+'s for the $\Theta^+(\frac{1}{2}^+)$((a),(b),(c)) and F_i^- for the $\Theta^+(\frac{1}{2}^-)$((d),(e),(f)) in the $\gamma p \to \bar{K}^0\Theta^+$.

III. PARITY DETERMINATION FROM DIFFERENTIAL CROSS SECTION AND SPIN OBSERVABLES

A. Angular Distribution and Photon polarization asymmetry

We now analyze the angular distribution. The angular distribution is defined by

$$\frac{d\sigma}{d\Omega}^{\pm} = \frac{1}{4}\sum_{s,s'}\frac{|\boldsymbol{q}|}{|\boldsymbol{k}|}\left|\boldsymbol{J}^{\pm}\cdot\boldsymbol{\epsilon}_{\lambda}\right|^{2}. \tag{7}$$

Following the convention given in Ref. [32], we choose the photon momentum $\boldsymbol{k}$ in Eqs.(1) and (2) along the z-axis and take $(\boldsymbol{k}\times\boldsymbol{q})$ as the y-axis normal to the production plane in the CM frame. In this coordinate system the current is expressed in terms of the CGLN amplitudes and given as $\frac{1}{4}\left|\boldsymbol{J}^{\pm}\cdot\boldsymbol{\epsilon}_{\lambda}\right|^{2} = I^{+}(\theta)$, where

$$\begin{aligned}
I^{+}(\theta) &= |F_1^{+}|^2 + |F_2^{+}|^2 + 2\mathrm{Re}(F_1^{+*}F_2^{+})\cos\theta \\
&\quad + \sin^2\theta\left[\frac{1}{2}(|F_3^{+}|^2 + |F_4^{+}|^2) + \mathrm{Re}(F_1^{+*}F_4^{+} - F_2^{+*}F_3^{+} + F_3^{+*}F_4^{+}\cos\theta)\right], \\
I^{-}(\theta) &= |F_1^{-}|^2 + |F_2^{-}|^2 + 2\mathrm{Re}(F_1^{-*}F_2^{-})\cos\theta \\
&\quad + \sin^2\theta\left[\frac{1}{2}(|F_3^{-}|^2\sin^2\theta + |F_4^{-}|^2) - \mathrm{Re}(F_1^{-*}F_3^{-} - F_2^{-*}F_4^{-} + F_2^{-*}F_3^{-}\cos\theta)\right],
\end{aligned} \tag{8}$$

for each parity of the $\Theta^{+}(\frac{1}{2}^{\pm})$, respectively.

Figs. 4 and 5 show the results of the angular distribution of Eq.(7) estimated with coupling constants listed in Table. I. The solid lines in the figures are the contributions of the Born terms and the notations for other lines are the same as those of Fig. 1. In Fig. 4 the solid lines of $\gamma n \to K^{-}\Theta^{+}$ near threshold, i.e. at E_γ =1.8 GeV, show a typical s-wave kaon production of the Born terms for $\Theta^{+}(\frac{1}{2}^{+})$ and p-wave distribution for $\Theta^{+}(\frac{1}{2}^{-})$, respectively. These features are quite distinctive to each other. Note that these are indeed the consequences already predictable from eq.(4), regardless of any model calculations for the CGLN amplitude $F_i^{\pm}$ of eq.(8). Furthermore, since such contrasting features of $\gamma n \to K^{-}\Theta^{+}$ are not degraded by the model-dependence especially due to the K^{*} and K_1 contributions near threshold, $E_\gamma = 1.8$ GeV, the angular distribution near threshold in the case of $\gamma n \to K^{-}\Theta^{+}$ should provide useful informations on the parity of the Θ^{+} without using a polarized photon beam and/or other polarized observables for that purpose. For the process $\gamma p \to \bar{K}^{0}\Theta^{+}$ in Fig. 5, however, due to the s-wave nature of the currents for both parities in eq.(5), the angular distributions are expected to be isotropic and therefore are not sensitive to the sign of the Θ^{+} parity. Thus, for the case of $\gamma p \to \bar{K}^{0}\Theta^{+}$ we agree with Ref. [15] which claims that one should analyze the spin observables to distinguish between the positive and negative parity of the Θ^{+}. These analyses confirm our earlier discussions.

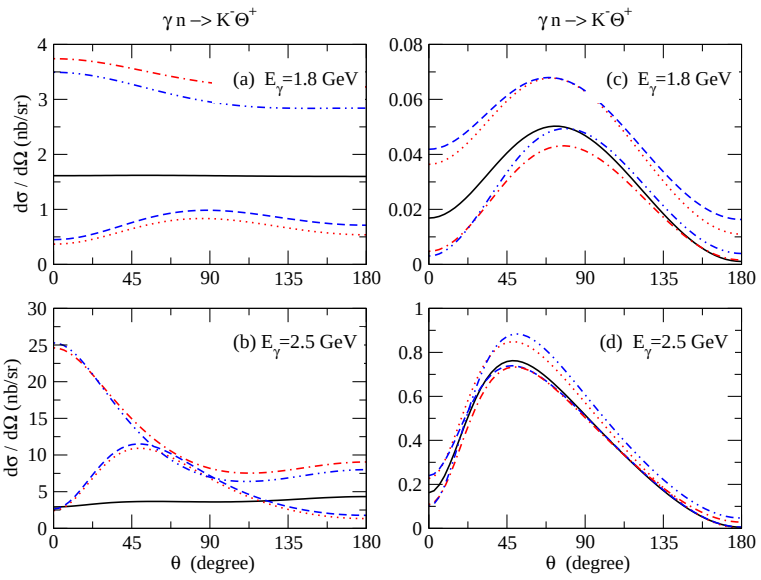

FIG. 4: (Color online) Angular distributions $\frac{d\sigma}{d\Omega}$ for $\gamma n \to K^- \Theta^+$ at $E_\gamma = 1.8$ and 2.5 GeV; (a), (b) for the $\Theta^+(\frac{1}{2}^+)$ and (c), (d) for the $\Theta^+(\frac{1}{2}^-)$. The notations for the curves are the same with those of Fig. 1.

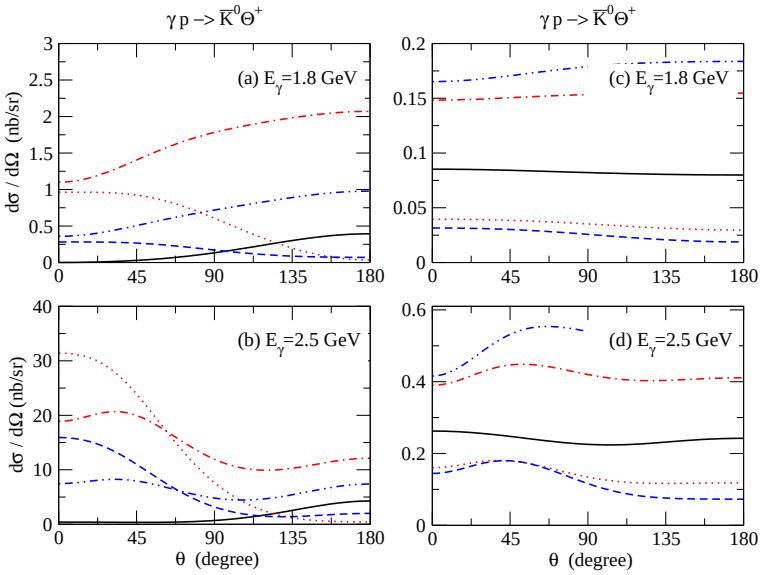

FIG. 5: (Color online) Angular distributions $\frac{d\sigma}{d\Omega}$ for $\gamma p \to \bar{K}^0 \Theta^+$ at $E_\gamma = 1.8$ and 2.5 GeV; (a), (b) for the $\Theta^+(\frac{1}{2}^+)$ and (c), (d) for the $\Theta^+(\frac{1}{2}^-)$. The notations for the curves are the same with those of Fig. 1.

It is natural to extend our analysis to the photon polarization asymmetry Σ. The asymmetry of photon polarization is defined by the difference between the x and y components of the current in the previous coordinate system. Thus the spin observable measures an interference between spin-flip and spin non-flip transitions. From eq.(4) different features depending on the parity of the Θ^+ can be expected in the measurement of the Σ for the $\gamma n \to K^- \Theta^+$ process. However,

the case of $\gamma p \to \bar{K}^0\Theta^+$ is not likely to give a definitive result in the measurement of Σ again as expected from eq. (5).

In the same coordinate system as before, the photon polarization asymmetry is defined by [32]

$$\Sigma = \frac{1}{4I(\theta)} tr\{J_y J_y^\dagger - J_x J_x^\dagger\}, \tag{9}$$

where the cartesian components of the currents $\boldsymbol{J}^{\pm}$ in this frame are given by

$$\begin{aligned} J_x^+ &= i(F_1^+ - F_2^+\cos\theta + F_4^+\sin^2\theta)\sigma_x + i\sin\theta(F_2^+ + F_3^+ + F_4^+\cos\theta)\sigma_z\,, \\ J_y^+ &= -F_2^+\sin\theta + i(F_1^+ - F_2^+\cos\theta)\sigma_y\,, \end{aligned} \tag{10}$$

for the $\Theta^+(\frac{1}{2}^+)$ and

$$\begin{aligned} J_x^- &= (F_2^- + F_4^-)\sin\theta + i(F_1^- + F_2^-\cos\theta - F_3^-\sin^2\theta)\sigma_y\,, \\ J_y^- &= -i(F_1^- + F_2^-\cos\theta)\sigma_x + iF_2^-\sin\theta\sigma_z\,, \end{aligned} \tag{11}$$

for the $\Theta^+(\frac{1}{2}^-)$, respectively.

With normalization by the angular distribution $I(\theta) = \frac{1}{4}(J_x J_x^\dagger + J_y J_y^\dagger)$, the results of the photon polarization asymmetry Σ are presented in Fig. 6 for $\gamma n \to K^-\Theta^+$ and Fig. 7 for $\gamma p \to \bar{K}^0\Theta^+$, respectively. In short, the polarization $\Sigma^{\pm}$ for $\gamma n \to K^-\Theta^+(\frac{1}{2}^{\pm})$ near threshold can be characterized

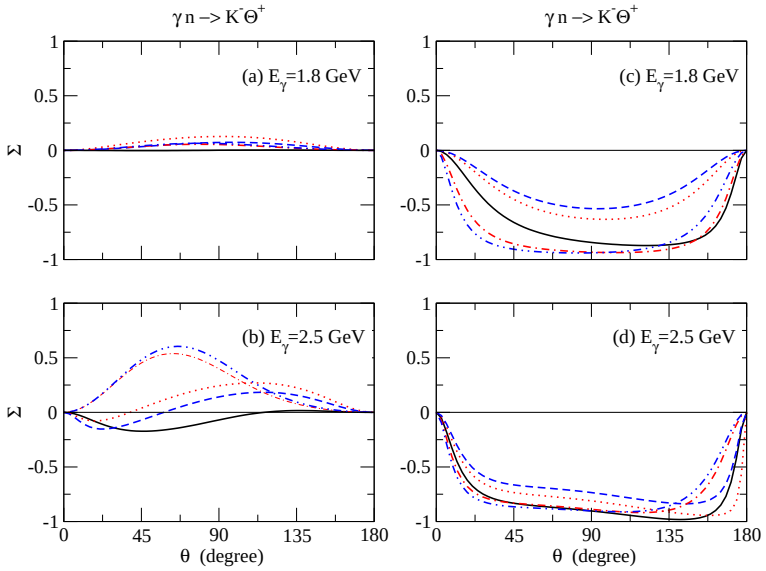

FIG. 6: (Color online) Polarization asymmetry of photon for $\gamma n \to K^-\Theta^+$ at $E_\gamma = 1.8$ and 2.5 GeV; (a), (b) for the $\Theta^+(\frac{1}{2}^+)$ and (c), (d) for the $\Theta^+(\frac{1}{2}^-)$. The notations for the curves are the same with those of Fig. 1.

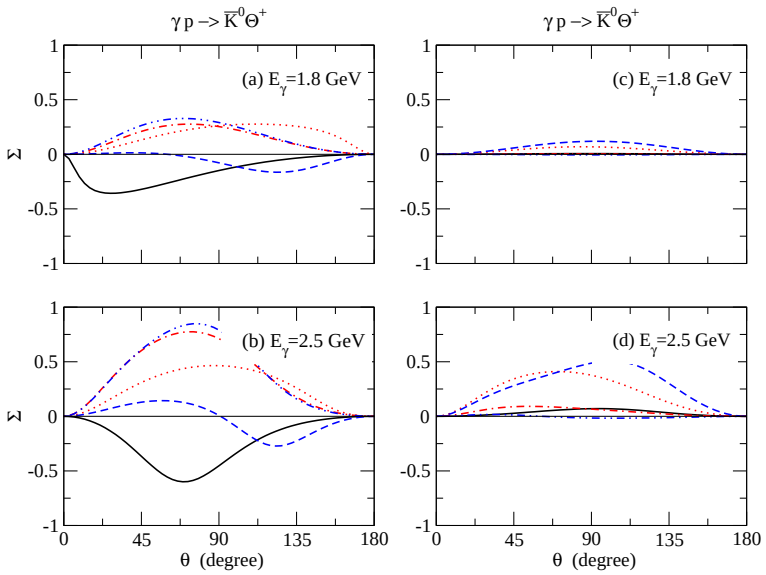

FIG. 7: (Color online) Polarization asymmetry of photon for $\gamma p \to \bar{K}^0\Theta^+$ at $E_\gamma = 1.8$ and 2.5 GeV; (a), (b) for the $\Theta^+(\frac{1}{2}^+)$ and (c), (d) for the $\Theta^+(\frac{1}{2}^-)$. The notations for the curves are the same with those of Fig. 1.

by such contrasting features between $\Sigma^+ \approx 0$ and $\Sigma^- \approx -1$. Note that these contrasting features are again the consequences of the conservation of parity and angular momentum plus threshold kinematics as discussed before. From Eqs. (10) and (11), the leading order contributions of F_1^+ and F_4^- for $\gamma n \to K^-\Theta^+$ near threshold lead to $J_x^+ \simeq iF_1^+\sigma_x$ and $J_y^+ \simeq iF_1^+\sigma_y$ for the $\Theta^+(\frac{1}{2}^+)$, and likewise, $J_x^- \simeq F_4^- \sin\theta$, $J_y^- \simeq 0$ for the $\Theta^+(\frac{1}{2}^-)$, respectively. Thus, $\Sigma^+ \approx 0$ can be accounted for by the strong cancellation of the spin-flip transition, while $\Sigma^- \approx -1$ resulted solely from the non-flip transition which could arise from the t-channel kaon exchange in the Born terms. Furthermore, such a distinction of Σ between the positive and negative parity of the Θ^+ near threshold is not much deteriorated by the model-dependent contributions of K^* and K_1. Therefore, observation of the photon polarization asymmetry Σ for the process $\gamma n \to K^-\Theta^+$ can also be a useful tool for determining the parity of the Θ^+.

For the process $\gamma p \to \bar{K}^0\Theta^+$, however, due to the dominance of F_1^+ and F_1^-, the currents in Eqs. (10) and (11) are approximated as $J_x^+ \simeq iF_1^+\sigma_x$ and $J_y^+ \simeq iF_1^+\sigma_y$ for the $\Theta^+(\frac{1}{2}^+)$ and $J_x^- \simeq iF_1^-\sigma_y$, $J_y^- \simeq -iF_1^-\sigma_x$ for $\Theta^+(\frac{1}{2}^-)$, respectively. Therefore, regardless of the Θ^+ parity, the polarizations $\Sigma^\pm$ are of the s-wave nature close to threshold and would be $\Sigma^\pm \approx 0$. In the case of the $\gamma p \to \bar{K}^0\Theta^+$ process we, thus, agree with Ref. [15] that one needs to measure more polarization observables beyond the single polarization Σ for a distinction between the $\Theta^+(\frac{1}{2}^+)$ and $\Theta^+(\frac{1}{2}^-)$.

It is worth to give a few remarks on our result in comparison with those of Ref. [14, 16, 33]. Zhao

[16] and Zhao and Al-Khalili [17] also carried out analyses of the single and double polarization observables of the process $\gamma n \to K^- \Theta^+$ with polarized photon beams using a quark potential model and examined kinematical and dynamical aspects for the purpose of determining the spin and parity of the Θ^+. Although the model in Ref. [16] is different from ours, we found that our results are rather close to the results of Ref. [16] in some cases supporting our findings in this work, i.e., dominance of the s-wave, and the p-wave nature near threshold depending on the parity of the Θ^+, respectively. In particular, our result of the photon polarization Σ is consistent with the corresponding result in Ref. [16]. Note that the sign convention adopted in Ref. [16] is opposite to ours due to the redefinition of Σ_A to Σ_W. Refs. [14, 33] also investigated the photon polarization Σ for the purpose of determining the parity of the Θ^+. For the model-independent analysis, Ref. [14] exploited the reflection symmetry of the photoproduction current, which states that the Pauli spin structure of J_x^+ is the same as that of J_y^-, and, likewise, the spin structure of J_y^+ as that of J_x^-. As can be seen in Eqs. (10) and (11), our analysis satisfies the same reflection symmetry that was presented in Ref. [14]. If the reflection symmetry is preserved in the threshold region, then, the invariance of each component of the current under an interchange of the parity would make the determination of the Θ^+ parity obscure just like in the case of $\gamma p \to \bar{K}^0 \Theta^+$ due to the similar shape of $\Sigma^\pm$ between the positive and negative parity. In the $\gamma p \to \bar{K}^0 \Theta^+$ process, the symmetric relation between the components of $J^\pm_{x(y)}$ are preserved and thus our result of not being able to distinguish the Θ^+ parity in this process is consistent with the result of Ref.[14].

B. Polarization asymmetries of target nucleon and recoiled Θ^+

In the previous section, we have demonstrated that due to the s-wave nature of both parities in the case of the $\gamma p \to \bar{K}^0 \Theta^+$, it is difficult to determine the parity of the Θ^+ from the measurement of angular distribution and photon polarization asymmetry. For a distinction of the Θ^+ parity in the $\gamma p \to \bar{K}^0 \Theta^+$ process, let us consider the polarization asymmetries of the target nucleon and recoiled Θ^+. We expect that these observables are also sensitive to the parity of the Θ^+ because the spin and parity of the initial state is highly correlated with those of the final state by the conservation laws. For instance, if the polarization of the Θ^+ in the $\gamma p \to \bar{K}^0 \Theta^+$ process is measured by the strong decay $\Theta^+ \to KN$, similar to the measurement of the Λ^0 polarization from the $\gamma p \to K^+ \Lambda^0$ process in Ref. [34], the decay of outgoing kaon should give different angular distributions between the two kinds of Θ^+ spin-parity $J^p = 1/2^+$ and $1/2^-$ in accordance with the partial wave of the KN state either p-, or s-wave multipole. Therefore determination of the

Θ^+ parity from these observables could be quite model-independent because such a correlation is independent of the dynamical details of the production phenomena. On the other hand, we note that the nonresonant Born terms except for the u-channel Θ^+ exchange could give little contribution since these observables are given by the imaginary part of the reaction amplitudes as shown below. Hence, the features of the observables depend pretty much on how one handles t-channel K^* and K_1 exchanges. The informations on the coupling constants of these particles are however currently not much available. With these in mind, we proceed to figure out how much the observables could be sensitive to the parity of the Θ^+, in particular in the case of $\gamma p \to \bar{K}^0\Theta^+$ process.

The polarization asymmetry of the target nucleon is the measurement of the nucleon spin polarization in the photoproduction process. It is defined by

$$T = \frac{d\sigma^+/d\Omega - d\sigma^-/d\Omega}{d\sigma^+/d\Omega + d\sigma^-/d\Omega}, \tag{12}$$

where the sign $+(-)$ represents that the spin polarization of the target nucleon is parallel(antiparallel) to the y-axis which is normal to the plane spanned by the $\boldsymbol{k} \times \boldsymbol{q}$ with the photon momentum $\boldsymbol{k}$ incident to the z-axis [32]. In this coordinate system, the target polarization asymmetries $T^\pm$ for each parity of the Θ^+ are given by the imaginary part of the CGLN amplitudes, i.e.,

$$\begin{aligned} T^+ &= \frac{\sin\theta}{I^+(\theta)} \mathrm{Im}[\, F_1^{+*}F_3^+ + F_2^{+*}F_4^+ + (F_1^{+*}F_4^+ + F_2^{+*}F_3^+)\cos\theta - F_3^{+*}F_4^+ \sin^2\theta\,], \\ T^- &= \frac{\sin\theta}{I^-(\theta)} \mathrm{Im}[\, F_1^{-*}F_4^- + F_2^{-*}F_4^- \cos\theta + (F_2^{-*}F_3^- - F_3^{-*}F_4^-)\sin^2\theta\,], \end{aligned} \tag{13}$$

respectively.

The polarization asymmetry of the recoiled Θ^+ is defined in the similar fashion, i.e.,

$$P = \frac{d\sigma^{(+)'}/d\Omega - d\sigma^{(-)'}/d\Omega}{d\sigma^{(+)'}/d\Omega + d\sigma^{(-)'}/d\Omega}, \tag{14}$$

but the sign $(+)'((-)')$ in this case represents that the spin polarization of the Θ^+ is parallel(antiparallel) to the y'-axis normal to the plane spanned by the direction of $\boldsymbol{k} \times \boldsymbol{q}$ with the scattered kaon momentum $\boldsymbol{q}$ directed to the z'-axis [32]. In this coordinate system, the polarizations $P^\pm$ are given by the following expressions in terms of CGLN amplitude for each parity of the Θ^+ respectively,

$$\begin{aligned} P^+ &= \frac{\sin\theta}{I^+(\theta)} \mathrm{Im}[\, F_1^{+*}(2F_2^+ - F_3^+ - F_4^+\cos\theta) - F_2^{+*}(F_3^+\cos\theta + F_4^+) + F_3^{+*}F_4^+\sin^2\theta\,], \\ P^- &= \frac{\sin\theta}{I^-(\theta)} \mathrm{Im}[\, 2F_1^{-*}F_2^- + F_1^{-*}F_4^- + F_2^{-*}F_4^-\cos\theta + (F_2^{-*}F_3^- - F_3^{-*}F_4^-)\sin^2\theta\,]. \end{aligned} \tag{15}$$

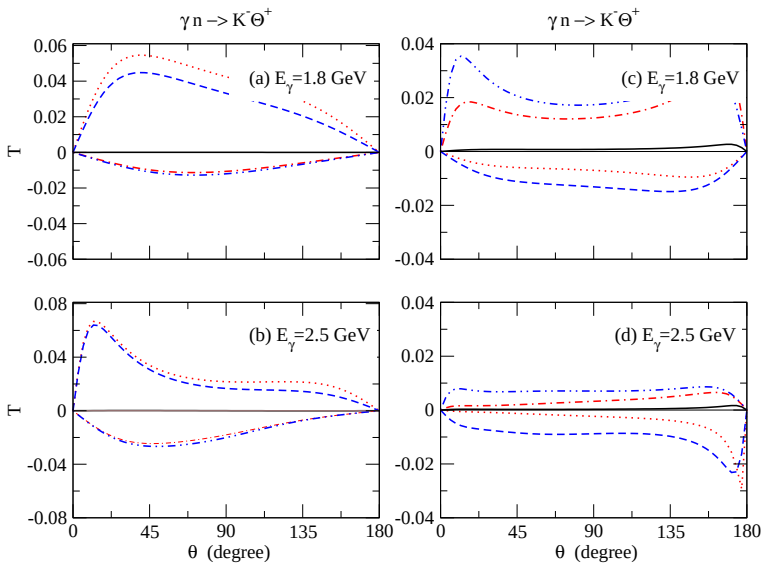

FIG. 8: (Color online) Polarization asymmetry of target T for $\gamma n \to K^- \Theta^+$ at $E_\gamma = 1.8$ and 2.5 GeV; (a), (b) for the $\Theta^+(\frac{1}{2}^+)$ and (c), (d) for the $\Theta^+(\frac{1}{2}^-)$. The notations for the curves are the same with those of Fig. 1.

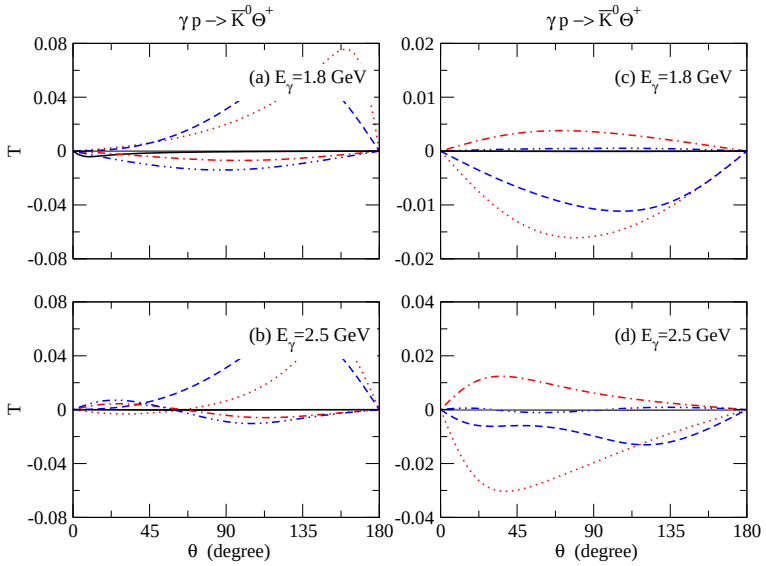

FIG. 9: (Color online) Polarization asymmetry of target T for $\gamma p \to \bar{K}^0 \Theta^+$ at $E_\gamma = 1.8$ and 2.5 GeV; (a), (b) for the $\Theta^+(\frac{1}{2}^+)$ and (c), (d) for the $\Theta^+(\frac{1}{2}^-)$. The notations for the curves are the same with those of Fig. 1.

We present the results of the target polarization T in Fig. 8 for $\gamma n \to K^- \Theta^+$ and in Fig. 9 for $\gamma p \to \bar{K^0} \Theta^+$, respectively. For the polarization asymmetry P, we show the results in Figs. 10 and 11 for $\gamma n \to K^- \Theta^+$ and $\gamma p \to \bar{K^0} \Theta^+$, respectively. In these figures, we see that the given expressions in Eqs. (13) and (15) provide general rules for T and P similar to Σ, i.e., they are

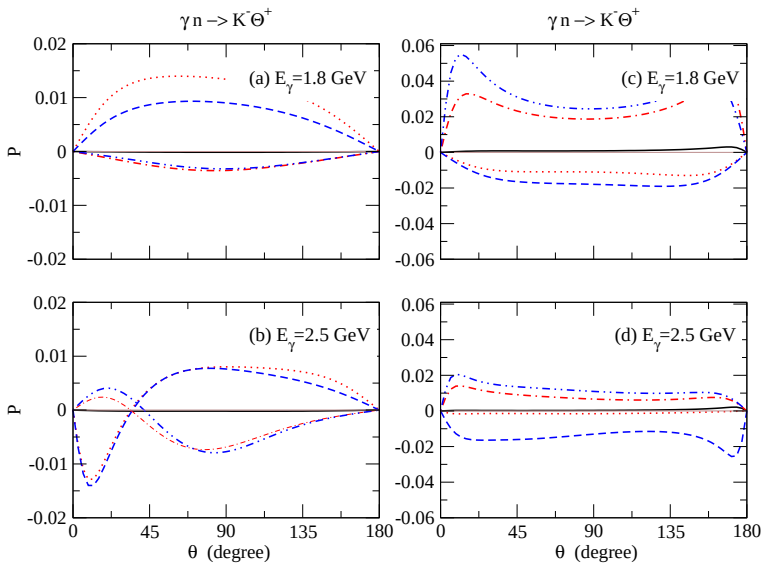

FIG. 10: (Color online) Polarization asymmetry of recoiled Θ^+ P for $\gamma n \to K^-\Theta^+$ at $E_\gamma = 1.8$ and 2.5 GeV; (a), (b) for the $\Theta^+(\frac{1}{2}^+)$ and (c), (d) for the $\Theta^+(\frac{1}{2}^-)$. The notations for the curves are the same with those of Fig. 1.

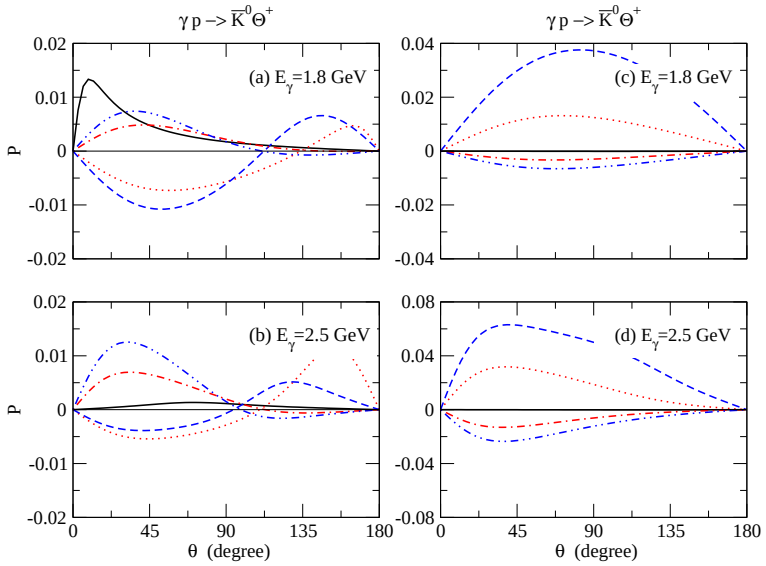

FIG. 11: (Color online) Polarization asymmetry of recoiled Θ^+ P for $\gamma p \to \bar{K}^0\Theta^+$ at $E_\gamma = 1.8$ and 2.5 GeV; (a), (b) for the $\Theta^+(\frac{1}{2}^+)$ and (c), (d) for the $\Theta^+(\frac{1}{2}^-)$. The notations for the curves are the same with those of Fig. 1.

identical to zero at $\theta = 0^\circ$ and 180° due to the dependence on the gross factor of $\sin\theta$. Moreover, as the CGLN amplitudes of the K^* and K_1 given by eqs. (3) and (6) do not depend on the angle significantly near threshold, the features of these observables at $E_\gamma = 1.8$ GeV exhibit the predominating $\sin\theta$ behavior with their signs reversed depending on the signs of the K^* and K_1

coupling constants. As shown in Figs. 8 and 9, it is interesting to see that the sign of target polarization T becomes opposite to each other whenever the parity of Θ^+ is changed, and this feature is common to both processes $\gamma n \to K^- \Theta^+$ and $\gamma p \to \bar{K}^0 \Theta^+$. Furthermore, as shown in Figs. 10 and 11, the Θ^+ polarization P also shows the pattern very similar to the case of polarization T. Thus, we find that the observables T and P are highly sensitive to the Θ^+ parity.

In addition we suppose that the features of the spin observables aforementioned would be less

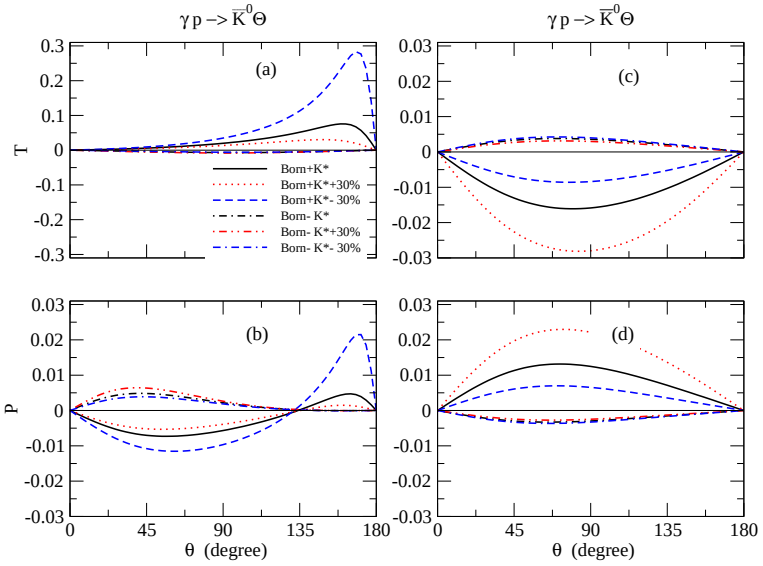

FIG. 12: (Color online) Dependence of polarization asymmetries T and P on the coupling constant $g_{K^*N\Theta}$ for $\gamma p \to \bar{K}^0 \Theta^+$ at $E_\gamma = 1.8$ GeV; (a), (b) for the $\Theta^+(\frac{1}{2}^+)$ and (c), (d) for the $\Theta^+(\frac{1}{2}^-)$. $g_{KN\Theta}$ is fixed in any case as given in Table I and contribution of K_1 is neglected for simplicity. Note that the notations for the curves are completely different from those in Figs. 8 - 11. The solid lines(the dotted lines of Figs. 9 and 11) are the sum of the Θ^+ pole term and K^* exchange with coupling constants given in Table I. Other lines correspond to the cases when the K^* coupling constant in the solid line increases, or decrease its value by 30% as denoted by the legend in this figure.

dependent on the K^* and K_1 coupling constants near threshold, because they are, by definition, given by the ratios normalized by differential cross section. This point should be clarified, however. In order to see the model-dependence of the T and P on the coupling constants of vector mesons, we reproduce these observables by changing the coupling constants $g_{K^*N\Theta}$, and $g_{K_1N\Theta}$ by an amount of 30% increase or decrease. The results are shown in Figs. 12 and 13. As a reference, the solid line is presented in the figure with coupling constants $g_{KN\Theta} = 0.984(0.137)$, $g_{K^*N\Theta} = 1.704(0.08)$ fixed from Table I. Other lines correspond to the cases when the coupling constant of the K^* is changed by 30% larger, or smaller than the solid line. Since the role of K_1 by such a change is

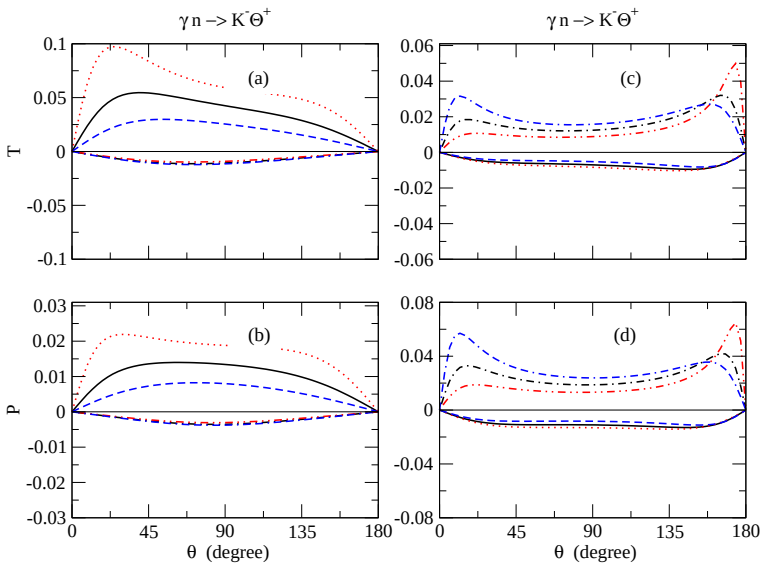

FIG. 13: (Color online) Dependence of polarization asymmetries T and P on the coupling constant $g_{K^*N\Theta}$ for $\gamma n \to K^-\Theta^+$ at $E_\gamma = 1.8$ GeV; (a), (b) for the $\Theta^+(\frac{1}{2}^+)$ and (c), (d) for the $\Theta^+(\frac{1}{2}^-)$. $g_{KN\Theta}$ is fixed in any case as given in Table I and contribution of K_1 is neglected for simplicity. The solid lines(the dotted lines of Figs. 8 and 10) are the sum of the Θ^+ pole term and K^* exchange with coupling constants given in Table I. Other lines correspond to the cases when the K^* coupling constant in the solid line increases, or decrease its value by 30% as denoted by the legend in Fig. 12 above. The notations for the curves are the same with those of Fig. 12

not significant, the contribution of K_1 is neglected in the figures for simplicity. As can be seen in the figures, the change of K^* coupling constant will not alter the contrasting features between the positive and negative parity of the Θ^+. Thus, the decisive features of the spin observables T and P are not affected significantly by the uncertainty of the $g_{K^*N\Theta}$. Conclusively, the measurement of spin observables T and P can help determine the parity of the Θ^+ in the future experiment especially from the $\gamma p \to \bar{K}^0\Theta^+$ process, which is more accessible than the neutron target.

IV. SUMMARY AND DISCUSSION

In this work, we have analyzed the unpolarized angular distribution and single polarization observables for the $\gamma N \to K\Theta^+$ process. Our analysis illustrates that the amplitude of $\gamma n \to K^-\Theta^+$ near threshold is characterized by the dominance of the s-wave (p-wave) multipole for the positive (negative) parity of the Θ^+. For the $\gamma n \to K^-\Theta^+$ process, therefore, measurements of unpolarized angular distribution and photon polarization asymmetry can be utilized for the determination of the Θ^+ parity. However, the situation becomes quite different in the case of

$\gamma p \to \bar{K}^0\Theta^+$ process because the direct coupling of photon to neutral $\bar{K}^0$ meson is absent. Due to the s-wave nature common to both parities of the Θ^+, measurements of such observables for $\gamma p \to \bar{K}^0\Theta^+$ near threshold are not so effective to reveal a distinction between the two opposite parities of the Θ^+. As usual in physical processes, the symmetry and the dynamics are strongly correlated to each other in the case of these observables. Taking into account the threshold kinematics of CGLN amplitude, we further confirm that the features of angular distribution and photon polarization asymmetry near threshold are natural consequences of the first principle conservation laws of parity and angular momentum. For determination of the Θ^+ parity using the $\gamma p \to \bar{K}^0\Theta^+$ process, we investigated the polarization asymmetries of target and recoiled Θ^+ and found out that these observables could serve for such purpose. The measurement of the spin-dependent observables near threshold should be encouraged, with special emphasis placed on the conservation laws and the threshold kinematics for model-independent determination of the Θ^+ parity.

Acknowledgments

This work was supported by a grant from the U.S. Department of Energy (DE-FG02-96ER 40947). CRJ thanks to the hospitality provided by the Department of Physics at Seoul National University where he took a sabbatical leave for the spring semester of the year 2005 and completed this work.

---

[1] A. V. Manohar, Nucl. Phys. B **248**, 19 (1984).
M. Chemtob, Nucl. Phys. B **256**, 600 (1985).
D. Diakonov, V. Petrov, and M. Polyakov, Z. Phys. A **359**, 305 (1997).

[2] LEPS Collaboration, T. Nakano *et al.*, Phys. Rev. Lett. **91**, 012002 (2003).

[3] SAPHIR Collaboration, J. Barth *et al.*, Phys. Lett. B **572**, 127 (2003).

[4] CLAS Collaboration I, S. Stepanyan *et al.*, Phys. Rev. Lett. **91**, 252001 (2003).
CLAS Collaboration II, V. Kubarovsky *et al.*, Phys. Rev. Lett. **92**, 032001 (2004).
DIANA Collaboration, V. V. Barmin *et al.*, Phys. Atom. Nucl. **66**, 1715 (2003).
A. E. Asratyan, A. G. Dolgolenko, and M. A. Kubantsev, hep-ex/0309042.
HERMES Collaboration, A. Airapetian *et al.*, Phys. Lett. **B 585**, 213 (2004).
ZEUS Collaboration, ZEUS Collaboration, Phys. Lett. **B 591**, 7 (2004).
COSY-TOF Collaboration, M. Abdel-Bav *et al.*, Phys. Lett. **B 595**, 127 (2004).
SVD Collaboration, A. Aleev *et al.*, hep-ex/0401024.

[5] BES, J. Z. Bai *et al.*, hep-ex/0402012.
Belle, K. Abe *et al.*, hep-ex/0409010.
BaBar, The BaBar Collaboration, hep-ex/0408064.
HERA-B, K. T. Knoepffe *et al.*, hep-ex/0403020.
CDF, D. O. Litvintsev *et al.*, hep-ex/0410024.
PHENIX, C. Pinkerton *et al.*, J. Phys. G**30**, S1201 (2004); nucl-ex/0404001.
LEP, S. R. Amstrong, hep-ex/0410080.
ALEPH, S. Schael *et al.*, Phys. Lett. B **599**, 1 (2004)
SPHINX, Yu. M. Antipov *et al.*, Eur. Phys. J. A**21**, 455 (2004).
HyperCP, M. J. Longo *et al.*, Phys. Rev. D **70**, 111101 (2004); hep-ex/0410027.
FOCUS, K. Stenson *et al.*, hep-ex/0412021.
Belle, R. Mizuk *et al.*, hep-ex/0411005.

[6] CLAS Collaboration, M. Battaglieri, R. D. Vita, V. Kubarovsky, D. Weygand and the CLAS Collaboration, talk presentation in the APS Meeting, Tampa, Florida, April 16, 2005.

[7] M. Karliner, and H. J. Lipkin, hep-ph/0506084.

[8] International Workshop Pentaquark 2004, SPring8, Japan, July 20-30, 2004.
International Conference on QCD and Hadronic Physics, Beijing, China, June 16-20, 2005.

[9] R. Jaffe and F. Wilczek, Phys. Rev. Lett. **91**, 232003 (2003).
D. Borisyuk, M. Faber, and A. Kobushkin, hep-ph/0307370.
B. K. Jennings and K. Maltman, Phys. Rev. D **69**, 094020 (2004).
C. E. Carlson, C. D. Carone, H. J. Kwee, and V. Nazaryan, Phys. Lett. B **573**, 101 (2003); Phys. Lett. B **579**, 52 (2004).
Fl. Stancu and D. O. Riska, Phys. Lett. B **575**, 242 (2003).
A. Hosaka, Phys. Lett. B **571**, 55 (2003).
L. Ya. Golzman, Phys. Lett. B **575**, 18 (2003); hep-ph/0309092.
M. karliner and H. J. Lipkin, Phys. Lett. B **575**, 249 (2003).

[10] S.-L. Zhu, Phys. Rev. Lett. **91**, 232002 (2003).
R. D. Matheus, F. S. Navarra, M. Nielsen, R. da Silva, and S. H. Lee, Phys. Lett. B **578**, 323 (2003).
J. Sugiyama, T. Doi, and M. Oka, Phys. Lett. B **581**, 167 (2004).
F. Csikor, Z. Fodor, S. D. Katz, and T. G. Kovács, JHEP 0311, 070 (2003); hep-lat/0309090.
S. Sasaki, hep-lat/0310014.

[11] A. W. Thomas, K. Hicks, and A. Hosaka, Prog. Theor. Phys. **111**, 291 (2004).

[12] C. Hanhart, M. B*ü*scher, W. Eyrich, K. Kilian, U.-G. Mei*β*ner, F. Rathmann, A. Sibirtsev, and H. Str*ö*her, Phys. Lett. B **590**, 39 (2004); hep-ph/0407107.

[13] C. Hanhart, J. Haidenbauer, K. Nakayama, U.-G. Mei*β*ner, hep-ph/0407107.

[14] K. Nakayama and W. G Love, Phys. Rev. C **70**, 012201 (2004); hep-ph/0404011.

[15] M. P. Rekalo, and E. Tomasi-Gustafsson, J. Phys. G**30**, 1459 (2004); hep-ph/0401050.

[16] Q. Zhao, Phys. Rev. D **69**, 053009 (2004).

[17] Q. Zhao and J. S. Al-Khalili, Phys. Lett. B **585**, 91 (2004).

[18] D. Drechsel, and L. Tiator, J. Phys. G**18**, 449-497 (1992).

[19] A. Donnachie, High Energy Physics vol.**v**, (edited by E. H. S. Burhop) Academic Press, 1972.

[20] O. Hanstein, D. Drechsel, and L. Tiator, Nucl. Phys. A **632**, 561 (1998).
M. Fuchs *et al.*, Phys. Lett. B **368**, 20 (1996).

[21] B. G. Yu, T. K. Choi, and C.-R. Ji, Phys. Rev. C **70**, 045205 (2004); nucl-th/0312075.

[22] S. Nussinov, hep-ph/0307357.
A. Casher, S. Nussinov, Phys. Lett. B **578**, 124 (2004).

[23] F. E. Close, and J. J. Dudek, Phys. Lett. B **586**, 75 (2004).

[24] C. E. Carlson, C. D. Carone, H. J. Kwee, and V. Nazaryan, hep-ph/0312325.

[25] C. E. Carlson, C. D. Carone, H. J. Kwee, and V. Nazaryan, Phys. Lett. B **573**, 101 (2003).

[26] http://pdg.lbl.gov/pdg.html

[27] R. A. Williams *et al.*, Phys. Rev. C **46**, 1617 (1992).

[28] K. Haglin, Phys. Rev. C **50**, 1688 (1994).

[29] C. F. Chew, M. L. Goldberg, R. E. Low, and Y. Nambu, Phys. Rev. **106**, 1345 (1957).

[30] B. Kerbikov, and F. Tabakin, Phys. Rev. C **62**, 064601 (2000).

[31] E. Marco, E. Oset, and H. Toki, Phys. Rev. C **60**, 015202 (1999).

[32] C. G. Fasano, F. Tabakin, and B. Saghai, Phys. Rev. C **46**, 2430 (1992).

[33] K. Nakayama and K. Tsushima, Phys. Lett. B **583**, 269 (2004); hep-ph/0311112.

[34] K. H. Glander *et al.*, Eur. Phys. J. A**19**, 251 (2004).